ELSEVIER

Biochimica et Biophysica Acta 1192 (1994) 167–176

BBA Biochimica et Biophysica Acta

Phase behavior of the antineoplastic ether lipid 1-*O*-octadecyl-2-*O*-methyl-glycero-3-phosphocholine

Norbert Maurer [a,*], Elmar Prenner [b], Fritz Paltauf [b], Otto Glatter [a]

[a] *Institute of Physical Chemistry, University of Graz, Heinrichstr. 28, A-8010 Graz, Austria*
[b] *Institute of Biochemistry and Food Chemistry, Technical University of Graz, A-8010 Graz, Austria*

(Received 17 November 1993)

Abstract

The physicochemical properties of the antineoplastic etherphospholipid 1-*O*-octadecyl-2-*O*-methyl-glycero-3-phosphocholine were examined in the concentration range 1–35% (w/w) lipid, as a function of temperature (range −10°C to 40°C) and of different aqueous solvents by dynamic light scattering, small- and wide-angle X-ray scattering, differential scanning calorimetry and ultrasonic speed measurements. On cooling the lipid dispersion undergoes a phase transition near 6°C, transforming slowly from a micellar into a lamellar gel phase with interdigitating hydrocarbon chains. The lamellar repeat distance is nearly constant over the hydration range 65–90% buffer ($d = 5.09$–5.14 nm). The size of the micelles in terms of the hydrodynamic radius is 3.8 ± 0.1 nm, the polydispersity is low. Their average shape is spherical. The electron density distribution across the micelle gives 2.5 nm for the extension of the hydrocarbon chains and 1.5 nm for the polar moiety. The existence of micelles was verified up to a concentration of 35% lipid. Throughout this concentration range size and shape do not change significantly. The kinetics of formation of the low-temperature phase is slow on cooling, increasing with increasing concentration. Upon heating the phase behavior shows a hysteresis. The extended lamellar organizations start to break down into smaller aggregates near 3°C. The micellar phase is reformed near 20°C.

Key words: Antineoplastic; Ether lipid; Lipid polymorphism; Quasi-elastic light scattering; Small-angle X-ray scattering; X-ray scattering, small-angle

1. Introduction

1-*O*-Alkyl-2-*O*-methyl-glycerophosphocholine (lysolecithin analog, LLA), has long been known as a cytostatic compound acting on various cancer cell lines in vitro [1–3] and in tumor-bearing animals [4]. The mechanisms of action of this compound and of various analogs that have since been synthesized is different from the mechanisms of action of 'classical' cytostatic agents for which DNA is the target. The activity of this compound is mediated indirectly by stimulating cytotoxic properties of macrophages [5,6] and directly due to cytostatic and cytotoxic properties as well as the induction of differentiation in tumor cells. The molecular mechanisms involved remain poorly understood. LLAs were shown to act on membrane-bound enzymes [7] and interfere with phospholipid synthesis [8] and/or protein kinase C activation [9]. Recent results point to LLAs as antiviral drugs with activity against enzymes required for HIV reproduction [10]. Although LLAs have not yet reached the level of clinical application, several of such compounds, including 1-*O*-octadecyl-2-*O*-methyl-glycero-3-phosphocholine (OMGPC), showed promising results in clinical trials [11,12]. Targeting these drugs to distinct parts of the body is a challenging task. Detailed knowledge of the kind of aggregates formed by the compounds either alone or in combination with other lipids or drugs, is of importance for an

* Corresponding author. Fax: +43 316 32248.

Abbreviations: OMGPC, 2-*O*-octadecyl-2-*O*-methyl-*rac*-glycero-3-phosphocholine; LLA, lysolecithin analog; PBS, phosphate-buffered saline (saline: sodium chloride); EDTA, ethylenediaminetetraacetic acid; DLS, dynamic light scattering; SAXS, small-angle X-ray scattering; DSC, differential scanning calorimetry; PDDF, pair distance distribution function; $h = (4\pi/\lambda)\sin\theta$ is the scattering vector, λ the wavelength of the Cu-K_α radiation and 2θ the scattering angle; $\Delta\rho(r)$, electron density distribution; R_H, hydrodynamic radius.

SSDI 0005-2736(94)00052-Q

understanding of their behavior in a biological environment, i.e., body fluids (blood, lymph). For example, half-life in the circulation and preferential uptake by distinct organs greatly depend on particle size [13]. In spite of the promise that these compounds hold as anticancer drugs, their physicochemical behavior in aqueous media remains poorly characterized [14,15].

Information about the physicochemical behavior could be useful in the interpretation of biochemical data such as binding, stimulation or tumor activity studies and could facilitate the elucidation of the molecular mechanisms of LLA activity. Other important parameters in this context are heterogeneity after preparation, reproducibility of preparations and stability upon storage.

The aim of this work is to establish the micellar phase boundaries of OMGPC with respect to concentration and temperature and to characterize the individual phases using dynamic light scattering (DLS), X-ray scattering (small- and wide-angle) and complementary techniques.

2. Materials and methods

2.1. Materials

1-*O*-Octadecyl-2-*O*-methyl-*rac*-glycero-3-phosphocholine was synthesized by condensation of racemic 1-*O*-octadecyl-2-*O*-methyl-glycerol with 2-chloro-2-oxo-1,3,2-dioxaphospholane and subsequent treatment of the cyclic phosphate with trimethylamine under conditions similar to those described by Chandrakumar and Hajdu [16,17]. The lipid was chromatographically purified on silica and aluminium oxide. OMGPC was judged to be pure by the appearance of a single spot on the thin-layer chromatogram using the ternary solvent systems $CHCl_3/CH_3OH/H_2O$ (65 : 25 : 4, v/v) and $CHCl_3/CH_3OH/NH_3$ (65:25:5, v/v) in conjunction with iodine, H_2SO_4 and molybdate as visualizing reagents. In addition, a ^{13}C-NMR spectrum was recorded on a Bruker AM-360 FT-NMR spectrometer (solvent: $CHCl_3$). Reagents used for buffer preparation were purchased in the highest obtainable grade from Merck. The lipid concentration was determined by the phosphorus assay [18].

2.2. Sample preparation

Lipid and buffer were prewarmed to 40°C. OMGPC was dispersed in aqueous buffers intermittently vortexing for 10 s and incubating at 40°C till the dispersion appeared optically clear. The sample was left to equilibrate for about 12 h. The quality of the micellar preparations was routinely examined with DLS. The following buffers were used: 10 mM Tris (pH 7.4); PBS (9 mM KH_2PO_4, 30 mM Na_2HPO_4, 150 mM NaCl) (pH 7.2). If not otherwise mentioned Tris was used. Throughout, the concentrations are given in weight percent (% w/w).

2.3. Dynamic light scattering

DLS measurements were carried out at a scattering angle of 90°. The homemade goniometer is equipped with an argon ion laser (Spectra Physics, model 2020-03, 3 W, 514.5 nm) and an ALV-5000 correlator (ALV, Germany). Briefly, as particles move in solution due to their Brownian motion the light scattered by them fluctuates [19]. Thus the time dependence of the scattering intensity, represented by its correlation function, provides information on scatterer motion. If all particles are of the same size, the correlation function is a single exponential function. Its decay is governed by the diffusion coefficient which can be obtained after linearization by a series expansion, a so-called cumulant fit [20]. The first cumulant c_1 gives the z-average of the diffusion coefficient. The diffusion coefficient D is related through the Stokes-Einstein equation $D = kT/6\pi\eta R_H$ to the hydrodynamic radius R_H, the size of an equivalent compact sphere, where k is the Boltzmann constant, T is the absolute temperature and η is the viscosity of the solvent. For a polydisperse sample this quantity is a mean value putting weight on large particles (for a sphere I_{sca} is proportional to R^6). An idea about the width of the distribution is given by the second cumulant c_2, ordinarily the ratio c_2/c_1^2 (polydispersity index) is taken as a measure of polydispersity. Size distributions were obtained through an Laplace inversion of the correlation function [21,22]. The intensity distribution $D_i(r)$ reflects the intensity with which particles of a certain size contribute to the signal (see above). The correlation functions were plotted on a logarithmic scale. There, each particle size leads to a fast decaying sigmoidal curve. The bigger the particles, the bigger the shift to larger correlation times. DLS was used to determine mean size and size distributions.

2.4. Small-angle X-ray scattering

The SAXS experiments were performed on a Kratky compact camera (slit collimation) equipped with a thermostatted sample holder and a linear position sensitive detector (MBraun, PSD-50M). The scattering intensities are smeared by the finite dimensions of the primary beam, slit width and slit length and its wavelength distribution (Cu-K_β part of the radiation). Solvent and sample were measured several times. After normalization, averaging and subtraction of the solvent scattering, the data were corrected for instrumental broadening effects (desmeared) [23–25]. The micellar scatter-

ing curves for low concentrations were interpreted in terms of the corresponding pair distance distribution functions (PDDF). The PDDF represents a histogram of distances inside the particle weighted with the electron density differences and goes to zero at the maximum particle dimension. It is the convolution square (spatial correlation function) of the electron density distribution $\Delta\rho(r)$. The electron density distribution across the micelle was obtained by deconvolution of the PDDF [26–30]. The method employed assumes a centrosymmetrical structure (spherical, cylindrical or lamellar symmetry). It avoids the square-root operation on the intensities and consequently the phase problem. SAXS was used to obtain information on the size of the micelles, on their internal structure (polar/hydrocarbon chain region) and on the kind of phase formed at low temperatures.

2.5. Wide-angle X-ray diffraction

The lipid dispersions were centrifuged into glass capillaries and mounted on a four circle diffractometer with a temperature control unit. X-rays were generated in a Siemens rotating anode unit, monochromatized (graphit monochromator, Cu-K_α radiation) and point collimated onto the sample. The diffraction patterns were recorded on X-ray films (Polaroid 57, NSN 6750-00-079-7395). The film to sample distance was 12.2 ± 0.1 cm.

2.6. Ultrasonic speed measurements

The ultrasonic speed was measured with a Density & Sound Analyzer (DSA 48) from the Anton Paar (Austria). The time required for a short pulse (170 ns) to run through a well defined sample cell (volume 1 ml) is used to calculate the ultrasonic speed with an accuracy of ± 1 m/s. The ultrasonic speed depends on the adiabatic compressibility and the density of the sample. The compressibility of solutions is a function of the temperature and of solute properties. Changes of the ultrasonic speed upon changing the temperature were shown to correlate with phase transitions occurring in the sample [31]. Since the changes are very small we used the specific ultrasonic speed $S_{spec} = (S_{solu} - S_{solv})/S_{solv}$. Changes can be visualized best by taking the negative first derivative of the specific ultrasonic speed $-S' = -d(S_{spec})/dT$ and plotting it against the temperature.

2.7. Differential scanning calorimetry

Calorimetric measurements were performed with a Perkin-Elmer differential scanning calorimeter DSC 4 over the temperature range -10 to 40°C. The dispersions were examined after incubation for different times at -10°C at a heating rate of 3 C°/min. Cooling scans were performed at the same rate.

3. Results

3.1. Preparation of micelles

Initially, lipid dispersions were prepared at room temperature. DLS measurements, however, gave correlation functions with a fast and a slow decaying component, indicating two distinct populations of aggregates, i.e., micelles and larger aggregates. The more and larger, the closer to 20°C. The amount of larger aggregates decreases with increasing temperature of preparation and vanishes at 40°C. Therefore, further preparations were carried out at 40°C. The micellar dispersions do not change on storage at room temperature for months. Incubation of the sample at temperatures well above room temperature after storage for comparable times in the refrigerator does not lead to the reformation of clear dispersions, a fraction of the lipid remains insoluble (white flocs).

3.2. Size of the micelles as determined with DLS

The hydrodynamic radius of the micelles extrapolated to zero concentration as determined from the cumulant fit is $R_H = 3.8 \pm 0.1$ nm ($D_0 = 56.1 \cdot 10^{-12}$ m^2 s^{-1}). The micelles are fairly monodisperse in size as indicated by a polydispersity index of 3–6%. R_H does not change significantly at different temperatures (10°C–40°C) and in different solvents (Tris, PBS with physiological sodium chloride concentration as stated in Materials and methods; additionally, physiological sodium chloride solution alone and Tris-buffered

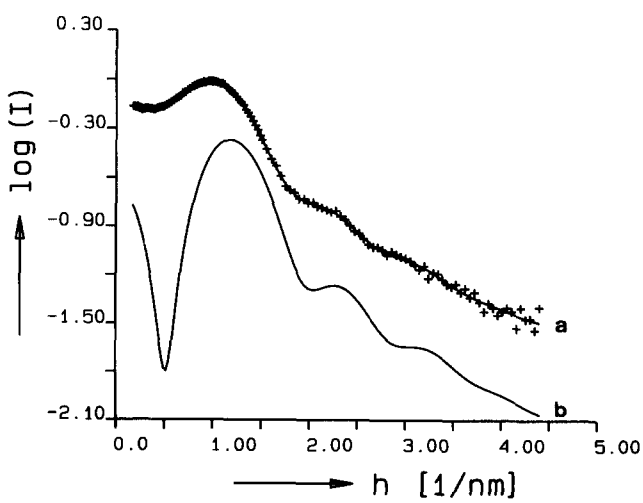

Fig. 1. Curve a: experimental scattering curve of a 1% dispersion at 20°C (crosses) and its approximation function (full line), range 0.177 nm$^{-1} \leq h \leq$ 4.404 nm^{-1}. Curve b: desmeared scattering curve.

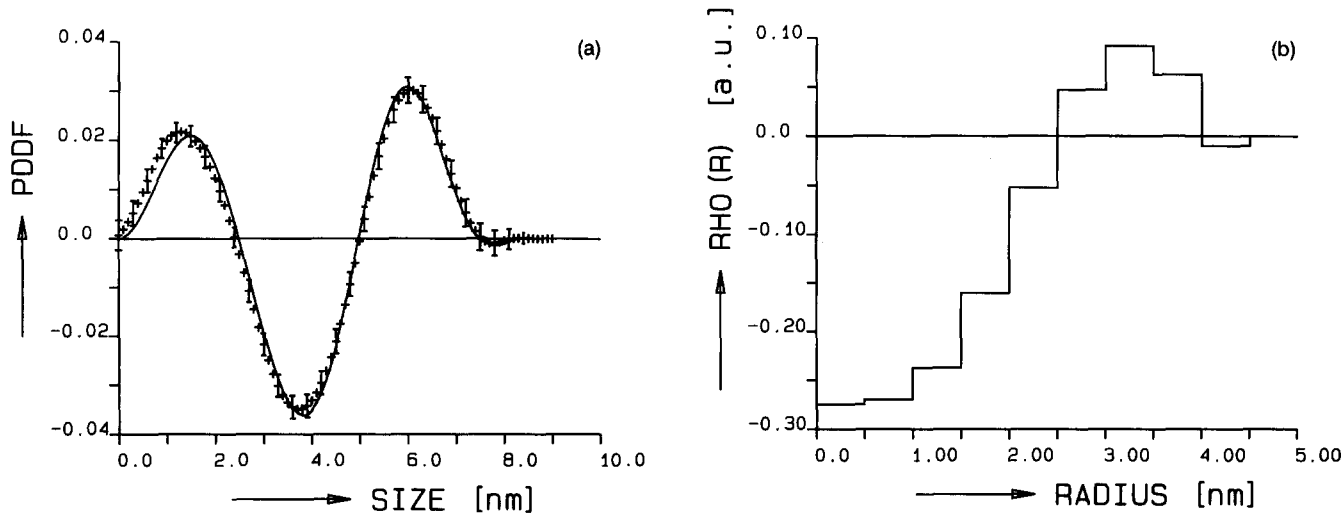

Fig. 2. (a) Pair distance distribution function (crosses) and the fit from the electron density profile (full line). (b) Radial electron density distribution calculated under the assumption of spherical symmetry as a sum of nine equidistant step functions.

potassium chloride (100 mM KCl) with 5 mM EDTA (pH ~ 6) were used).

3.3. Size, shape and internal structure as determined with SAXS

The experimental scattering curve of a 1% dispersion of OMGPC at 20°C (crosses) and its approximation function (full line) are depicted in the range 0.177 $nm^{-1} \leq h \leq 4.404\ nm^{-1}$ in Fig. 1a. The depression of the innermost part of the scattering curve is due to the low overall contrast of the micelles. Fig. 1b shows the desmeared scattering curve. In theory, the scattering curve of a spherical aggregate shows a series of pronounced side maxima separated by zeros. In practice we see only minima because the condition of spherical symmetry is never perfectly fulfilled in real systems. This leads to a smearing out of the maxima and minima.

The same information as in the scattering function, however, in a more straightforward form (real space), is given by its Fourier transform, the PDDF. The PDDF is depicted in Fig. 2a (crosses), the full line is the fit from the electron density profile (Fig. 2b). The maximum dimension of the micelles is approx. 7.7 nm. The negative part is a consequence of the electron density differences across the micelle (polar part and hydrocarbon region). Starting with the PDDF, the best centrosymmetrical electron density distribution $\Delta\rho(r)$ was calculated as a sum of 9 equidistant step functions (Fig. 2b). A brief comment on the meaning of the steps in the electron density distribution in order to avoid its

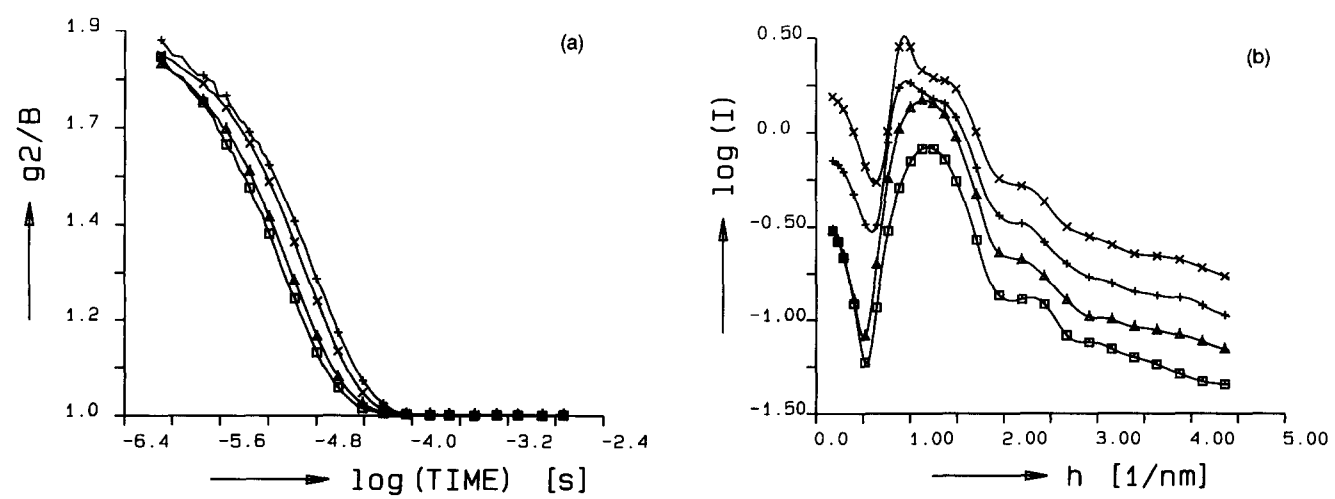

Fig. 3. (a) DLS: normalized intensity correlation functions as a function of concentration (1% (+), 10% (×), 25% (△) and 30% (□)). (b) SAXS: desmeared scattering curves for different OMGPC concentrations shifted by arbitrary factors (1% (□), 10% (△), 25% (+) and 30% (×), $T = 20°C$).

overinterpretation: The step width in the $\Delta\rho(r)$-distribution corresponds to the resolution of the PDDF (i.e., the distance of the knots of cubic B-splines). These steps are not independent, as neighboring steps are correlated by the stabilization procedure used in the deconvolution of the PDDF, i.e., they should not be misinterpreted as real steps representing details of the electron density distribution of the micelles. They just model the $\Delta\rho(r)$-function. A smooth profile running through these steps will give an eqivalent fit to the original PDDF. For details the reader is referred to the original literature [23,24,26–28]. The electron density distribution gives an idea about the extension of the polar region, approx. 1.5 nm, and the hydrocarbon moiety, approx. 2.5 nm. This procedure will not be able to fit the PDDF with reasonable accuracy, if the condition of spherical symmetry is not fulfilled. In our case the fit to the PDDF (Fig. 2a, full line) demonstrates a good agreement with the assumption of a spherical shape. The small deviations in the inner part are due to local electron density fluctuations (background).

3.4. Aggregation behavior as a function of concentration

The existence of micelles was verified with DLS and SAXS up to a concentration of 35% lipid.

(a) DLS. Generally, at higher concentrations the motion of each particle is influenced by other particles nearby. The intensity correlation functions (Fig. 3a) are shifted towards smaller correlation times and remain, however, unchanged in their decay behavior. The apparent diffusion coefficient increases linearly with concentration [32].

(b) SAXS. In the case of interacting spherical particles the scattering intensity $I(h)$ can be written as the product of the particle form factor $P(h)$ and the structure factor $S(h)$. $S(h)$ describes the interparticle interferences. For dilute solutions it is a constant. The SAXS curves in Fig. 3b show the development of a structure factor with a pronounced maximum for increasing concentrations, superposed on the micellar form factor. The position of the first maximum of the structure factor is related to the interparticle distance. The position and the number of side maxima of the form factor is preserved at all concentrations. This indicates that the micelles do not change significantly in size and shape. Further support of this is gained by the fact that a reasonable structure factor can be obtained by dividing the scattering curve by the form factor. As a first approximation the scattering curve of a 1% dispersion was taken as the form factor. Measurements at lower concentrations are difficult due to the low contrast. A detailed study of the micellar interactions, however, was neither intended nor is it possible on a slit collimating X-ray camera.

3.5. Aggregation behavior as a function of temperature

Phase transitions

Cooling down from 40°C to 0°C, a phase transition occurs near 6°C. This is evidenced by the increase in scattered light intensity at 90° (Fig. 4a) and the change of ultrasonic speed (Fig. 4b). The samples were cooled in 1°C increments with 20 min incubation time at each temperature. Optically, the initially clear dispersions become turbid and jellylike for low concentrations (< 10%) and white and stiff for high concentrations.

DSC experiments were performed to confirm the phase transition. Incubation of a 25% lipid dispersion at −10°C for 30 min gives on heating a small endothermic peak with the maximum at 2.5°C and two sharp endothermic peaks centered near 17 and 20°C (Fig.

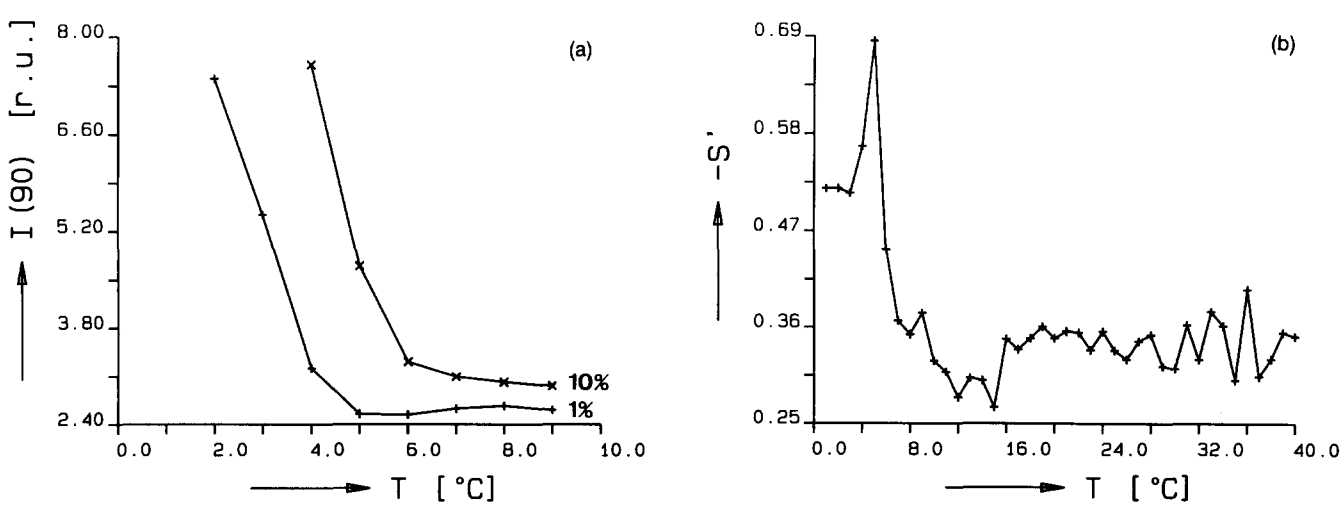

Fig. 4. (a) Intensity of light scattered at 90° as a function of temperature for different concentrations (1% (+), 10% (×)). (b) First derivative of the specific ultrasonic speed as a function of temperature (10%).

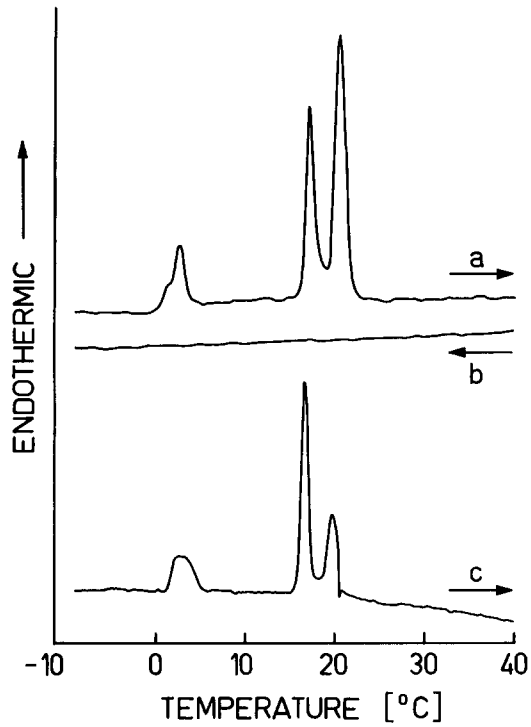

Fig. 5. DSC curves (heating and cooling rate 3 C°/min, 25% lipid). Curve a: heating scan after 30 min incubation at −10°C; curve b: cooling scan; curve c: heating scan after 4 h at −10°C.

5a). The 10% dispersion behaves identically, although with a much smaller low temperature peak. On cooling from 40°C to −10°C at a rate of 3 C°/min, no transition is detected by DSC (Fig. 5b). The 20°C peak decreases on prolonged incubation at −10°C for 4 h (Fig. 5c).

Fig. 6a is a plot of the intensity of light scattered at 90° of a 1% and a 5% dispersion as a function of time at constant temperature ($T = 2$°C). The intensity remains nearly constant for a certain period of time, which depends on the concentration. It is more than 2 h for a concentration of 1%, approx. 1 h for 5% and some minutes for concentrations greater than 20%. During this period only minor growth of the larger aggregates takes place. This initial lag time is followed by a steep increase in intensity, pointing to rapid growth of larger aggregates. The micellar peak decreases at the expense of larger aggregates as shown in Fig. 6b for the 5% lipid dispersion. The formation of the low temperature phase is a kinetically slow process, faster with increasing concentration.

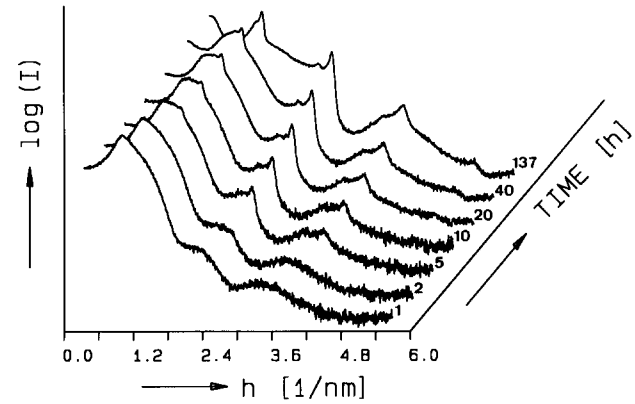

Fig. 7. Experimental scattering curves as a function of time at 0°C shifted by arbitrary factors for better visibility (after 1, 2, 5, 10, 20, 40 and 137 h, $c = 30\%$).

Kind of phase formed at low temperatures

The evolution of equidistantly spaced peaks in the experimental SAXS curves (Fig. 7, 30%) proves the lamellar nature of the phase formed. This pattern is representative for concentrations ≥ 10% and for different solvents (see Materials and methods). The curves

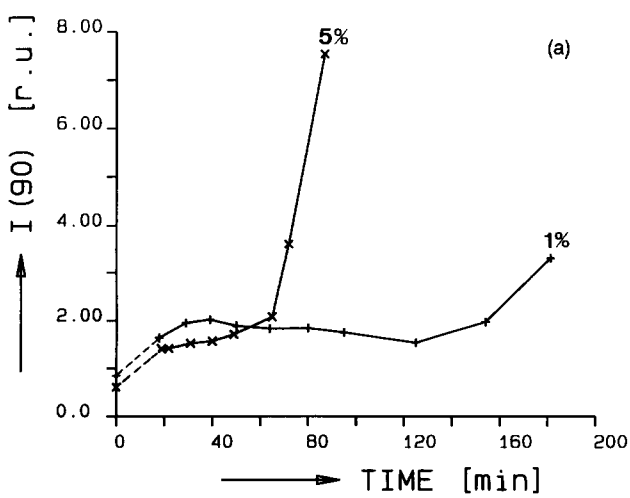

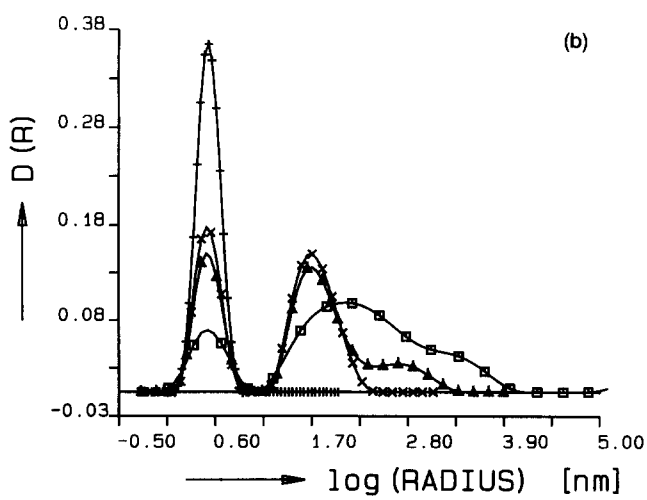

Fig. 6. (a) Intensity of light scattered at 90° as a function of time at 2°C (1% (+), 5% (×)). (b) Intensity distributions corresponding to selected time points of the 5% dispersion in Fig. 6a (1 (+), 20 (×), 40 (△) and 75 min (□)).

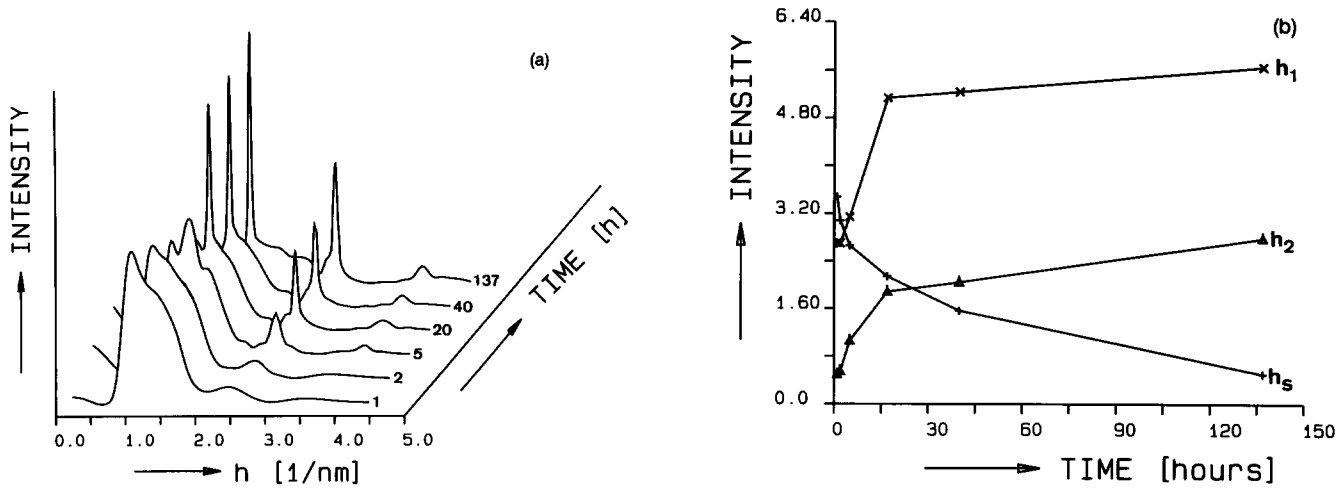

Fig. 8. (a) Desmeared scattering curves as a function of time at 0°C after 1, 2, 5, 20, 40 and 137 h, $c = 30\%$ (the curves are shifted by an arbitrary factor). (b) Development of the structure factor peak ($h_s = 0.935$ nm^{-1}, (+)) and the 1st (×) and 2nd (△) order lamellar peaks ($h_1 = 1.234$ nm^{-1}) of (a) as a function of time.

are smeared by collimation and wavelength effects. The small pre-peaks are due to the K_β line of the X-ray radiation. The desmeared scattering curves after 1, 2, 5, 20, 40 and 137 h at 0°C are depicted in Fig. 8a. The peak of the structure factor of the micelles at $h = 0.935$ nm^{-1} is decreasing at the expense of the first order lamellar diffraction peak at $h = 1.234$ nm^{-1} (Fig. 8b). At the same time higher lamellar diffraction orders are developing. The lamellar repeat distance d is 5.09 nm. It remains nearly constant in the hydration range of 90%–65% ($d = 5.14$–5.09 nm). Again, the conversion of the micellar to the lamellar phase is seen to be a slow process. It takes days to weeks to come to completion.

Reheating after incubation for several days at 0°C, the lamellar peaks start to degrade and broaden near 3°C and transform slowly into a scattering pattern typical for the micellar dispersions near 20°C (Fig. 9).

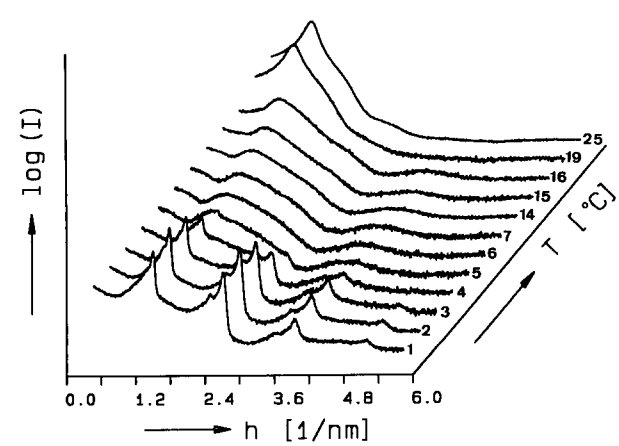

Fig. 9. Smeared scattering curves upon heating from 0°C to 25°C shifted by arbitrary factors (incubation at 0°C for 4 days, 35% lipid dispersion).

Optical inspection shows that the white gel becomes opaque and eventually clears up near 20°C.

The wide-angle diffraction pattern of a 30% dispersion at −10°C (Fig. 10) shows a single sharp symmetrical ring centered at $(4.3\ \text{Å})^{-1}$. The lipid dispersion was incubated for 4 h, the film was exposed for 14 h.

At concentrations below 10% the low temperature phase behaves rather peculiarly. In the beginning a

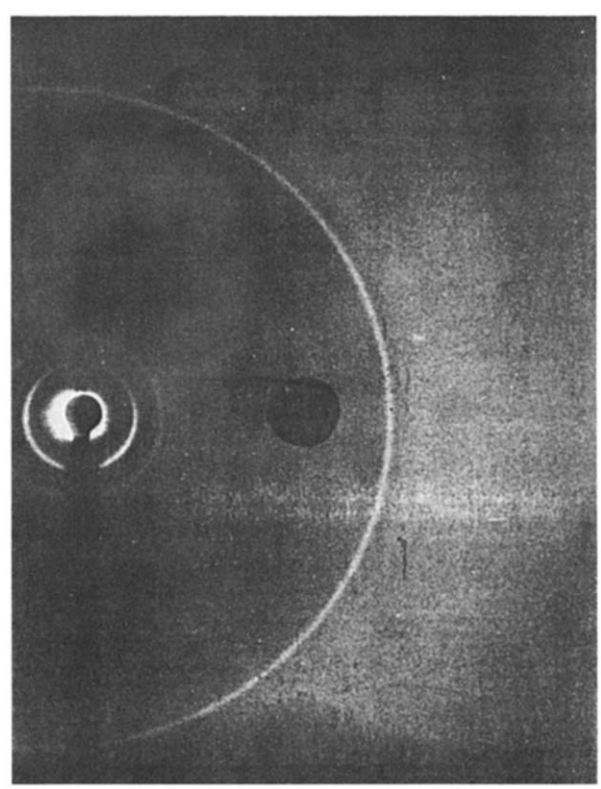

Fig. 10. X-ray wide-angle diffraction pattern of a 30% lipid dispersion at −10°C (incubation time 5 h, exposure time 14 h).

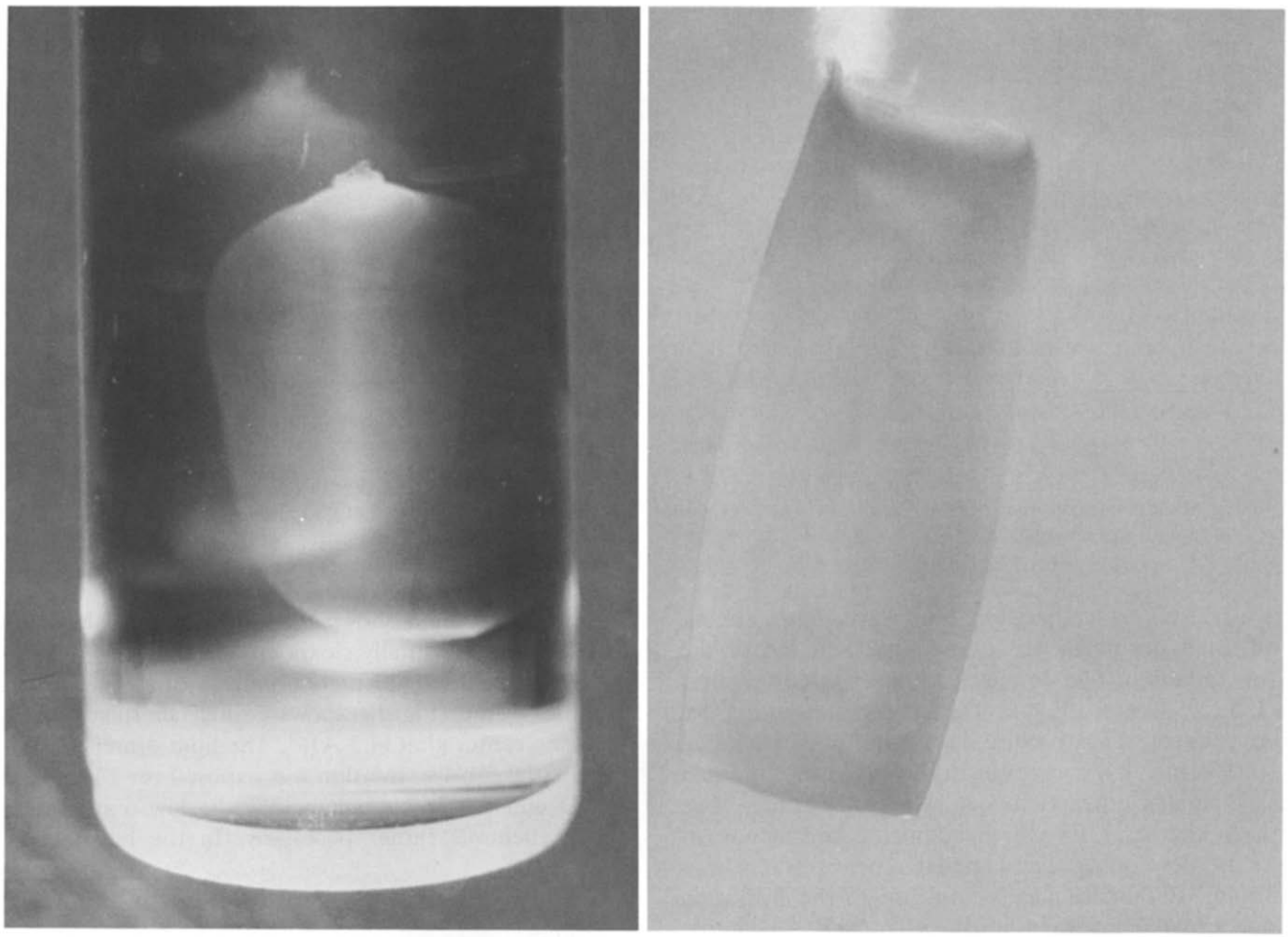

Fig. 11. Photographs of the cylinder formed at low concentrations after 20 h and more than 1 day at 1°C in a cylindrical cuvette (1% dispersion, 60 × magnification, the diameter of the cuvette is 1 cm).

turbid jellylike phase is formed, which is slowly contracting, leaving after more than a day a cylinder (cylindrical cuvette) in a clear supernatant solution. DLS size distributions (not shown) show that the latter is micellar with a small fraction of larger aggregates. Approx. 30% of the total amount of lipid is in the cylinder (phosphorus assay). Fig. 11 shows two photos of the cylinder taken after 20 h (left) and more than 1 day, respectively.

4. Discussion

In spite of their importance as antineoplastic substances and their potential in drug targeting, the physicochemical properties of ether lysolipid analogs have not yet been systematically investigated [15,33–35]. The corresponding ester lysolipids and their analogs have been the focus of more attention [36–42]. A micellar to lamellar phase transition at low temperatures was reported for all these compounds. Sample history was shown to affect not only the kinetics of this transition but also the kind of lamellar phase formed. While this transition and the lamellar phases formed have been studied in some detail, the characterization of the micellar phases was neglected.

Structurally, OMGPC is an amphiphile consisting of a long C_{18}-hydrocarbon chain in position 1 of the glycerol backbone, a short methyl group in position 2 and the phosphocholine headgroup in position 3. The relatively large headgroup together with the highly asymmetrical hydrocarbon tail region gives this molecule a 'cone' shaped appearance. This shape allows OMGPC to pack into micellar geometries [43]. DLS measurements show that the micelles are small and monodisperse. The hydrodynamic radius at infinite dilution is 3.8 ± 0.1 nm. This is in good agreement with a diameter of 7.7 nm from our SAXS data and micellar radii reported for n-octadecylphosphocholine determined with DLS, $R_H = 3.7 \pm 0.2$ nm [44] and 1-stearoyl-2-lyso-glycero-3-phosphocholine from NMR diffusion experiments with $R_H = 3.81$ nm [41]. The

electron density profile gives 2.5 nm for the length of the hydrocarbon chains and 1.5 nm for the polar region.

The phase transition characteristics of OMGPC depend on the thermal and temporal history of the sample. Upon cooling OMGPC undergoes a single kinetically slow transition from a micellar into a lamellar gel phase near 6°C. On heating DSC revealed a hysteresis. The low temperature transition centered at 2.5°C was followed by two additional transitions near 17°C and 20°C. The latter is decreasing with increasing incubation time at low temperatures and represents a metastable phase. Metastable states were also reported for n-octadecylphosphocholine [35] after prolonged incubation at low temperatures and for 1-stearoyl-2-lyso-glycero-3-phosphocholine [37] after too short preincubation at low temperatures. Structurally, the extended bilayers begin to break down upon heating into smaller aggregates, which transform into a micellar phase near 20°C (Fig. 9). The same sequence of heating transitions, lamellar gel below 9.2°C via medium-size vesicles to micelles above 18.4°C, is also reported for 1-*O*-octadecyl-2-acetyl-*sn*-glycero-3-phosphocholine [33,34]. 1-Stearoyl-2-acetyl-*sn*-glycero-3-phosphocholine shows two similar transitions at 6.5°C and 18.5°C [42] corresponding to a lamellar crystalline phase to lamellar gel phase transition (indirect evidence with Raman spectroscopy) and the subsequent formation of micelles. In both cases the behavior on cooling has not been investigated. For n-octadecylphosphocholine [35] the lamellar order started to degrade long before the lamellar to micellar transition indicated by DSC upon heating. The lysolipid in this series, 1-stearoyl-2-lyso-*sn*-glycero-3-phosphocholine, undergoes a single transition at 27°C from a lamellar gel phase to a micellar phase [36,39]. The process of conversion has not been studied. Due to the different methods and measuring protocols employed, the question wether a hysteresis is a general feature of the thermotropic phase behavior of these lipids or not cannot be answered unambiguously.

The low temperature phase is lamellar with a repeat distance of approx. 5.1 nm in excess 'water'. This can be realized only upon interdigitation and/or tilting of the hydrocarbon chains. By argument of geometrical reasons, effective packing of highly asymmetrical lipids, where the projected headgroup area is much larger than that of the tails, is only possible if the chains interdigitate [45]. Chain interdigitation was reported for a series of lysolipids and analogs [33,35,36,39]. In single crystals OMGPC molecules (D-configuration) pack in stacked bilayers with interdigitating head groups and interdigitating and tilting hydrocarbon chains [46]. The wide angle region of OMGPC shows a sharp symmetrical ring centered at $(4.3\ \text{Å})^{-1}$. This is indicative for hydrocarbon chains in the gel state. Increasing chain tilt produces an additional more diffuse wide angle reflection following the sharp reflection [47,48]. Our data give evidence that the lamellar phase we see consists of bilayers with interdigitated chains.

The kinetics of formation is slow (days to weeks), faster with increasing concentration. This is a common feature of lysolipids and analogs. DLS experiments (Fig. 6) show an initial lag time where only minor growth takes place, followed by rapid growth. The lag time was the shorter, the higher the concentration. On the other hand, evolution of long range order in the sense of the appearance of diffraction peaks took hours even for higher concentrations (> 10%) (Fig. 7). This behavior was also reported for 1-stearoyl-2-lyso-glycero-3-phosphocholine [36,38]. Wu and Huang [38] described the micellar to lamellar phase transition in terms of nucleation and growth (measurements of fluorescence anisotropy), i.e., (1) formation of lamellar aggregates (hydrocarbon packing rearrangement) and (2) growth of the aggregates to extended lamellar structures.

In dispersions with concentrations lower than 10% a phase separation into a clear micellar dispersion and a cylinder (cylindrical cuvette) occurs after incubation for more than 1 day at temperatures below 6°C. We do not yet have an explanation for this behavior.

Concluding, OMGPC forms spherical micelles which transform into a lamellar gel phase on cooling near 6°C. Reheating, the lamellar gel converts via smaller aggregates into micelles near 20°C. Since OMGPC is widely used in medical and biochemical studies, some practical aspects have to be stressed. For the sake of reproducibility of further experiments, preparations should be carried out at 40°C. Long-term storage of aqueous dispersions in the refrigerator is not recommended.

Acknowledgements

This work was supported by research grant P9214-TEC from the Fonds zur Förderung der Österreichischen Forschung. We thank Doz. Stelzer and his collaborators for the use of their DSC and Doz. Kratky and Karl Gruber for helpful assistance with the wide-angle measurements. In addition, we thank Herbert Stütz for his help with the purification of OMGPC and the determination of the phosphorus content.

References

[1] Mangold, H.K. and Paltauf, F. (1983) Ether Lipids: Biochemical and Biomedical Aspects, Academic Press, New York.
[2] Noseda, A., Berens, M.E., Piantadosi, C. and Modest, E. (1987) Lipids 22, 878–883.

[3] Berdel, W.E., Von Hoff, D.D., Unger, C., Schick, H.D., Fink, U., Reichert, A., Eibl, H. and Rastetter, J. (1986) Lipids 21, 301–304.
[4] Berger, M.R. and Schmähl, D. (1987) Lipids 22, 935–942.
[5] Berdel, W.E., Bausert, W.R., Weltzien, H.U., Modolell, M.L., Widmann, K.H. and Munder, P.G. (1980) Eur. J. Cancer 16, 1199–1204.
[6] Andreesen, R., Osterholz, J., Luckenbach, G.A., Costabel, U., Schulz, A., Speth, V., Munder, P.G. and Löhr, G.W. (1984) J. Natl. Cancer Inst. 72, 53–59.
[7] Powis, G., Seewald, M.J., Gratas, C., Riebow, J. and Modest, E.J. (1992) Cancer Res. 52, 2835–2840.
[8] Herrmann, D.B.J. and Neumann, H.A. (1986) J. Biol. Chem. 261, 7742–7747.
[9] Parker, J., Daniel, L.W. and Waite, M. (1987) J. Biol. Chem. 262, 5385–5393.
[10] Kucera, L., Iyer, N., Leake, E., Raben, A., Modest, E., Daniel, L. and Piantadosi, C. (1990) AIDS Res. Hum. Retroviruses 6, 491–501.
[11] Berdel, W.E., Fink, U. and Rastetter, J. (1987) Lipids 22, 967–969.
[12] Berdel, W.E. (1987) Lipids 22, 970–973.
[13] Cullis, P.R., Hope, M.J., Bally, M.B., Madden, T.D., Mayer, L.D. and Janoff, A.S. (1987) in Liposomes: From Biophysics to Therapeutics (Ostro, M.J., ed.), pp. 39–72, Marcel Dekker, New York.
[14] Weltzien, H.U., Arnold, B., Blume, A. and Kalkoff, H.G. (1976) Chem. Phys. Lipids 16, 267–275.
[15] Dick, D. and Lawrence, D.S. (1992) Biochemistry 31, 8252–8257.
[16] Chandrakumar, N.S. and Hajdu, J. (1981) Tetrahedron Lett. 22, 2949–2952.
[17] Chandrakumar, N.S. and Hajdu, J. (1982) J. Org. Chem. 47, 2144–2147.
[18] Broekhuyse, R.M. (1968) Biochim. Biophys. Acta 152, 307–315.
[19] Pecora, R. (1985) Dynamic Light Scattering, Plenum Press, New York.
[20] Koppel, D.E. (1972) J. Chem. Phys. 57, 4814–4820.
[21] Schnablegger, H. and Glatter, O. (1991) Appl. Opt. 30, 4889–4896.
[22] Glatter, O., Sieberer, J. and Schnablegger, H. (1991) Part. Part. Syst. Charact. 8, 274–281.
[23] Glatter, O. (1977) J. Appl. Cryst. 10, 415–421.
[24] Glatter, O. (1982) in Small-Angle X-Ray Scattering (Glatter, O. and Kratky, O., eds.), pp. 119–196, Academic Press, London.
[25] Glatter, O. and Gruber, K. (1993) J. Appl. Cryst. 26, 512–518.
[26] Glatter, O. (1981) J. Appl. Cryst. 14, 101–108.
[27] Glatter, O. and Hainish, B. (1984) J. Appl. Cryst. 17, 435–441.
[28] Glatter, O. (1988) J. Appl. Cryst. 21, 886–890.
[29] Glatter, O. (1991) Prog. Colloid. Polym. Sci. 84, 46–54.
[30] Maurer, N. and Glatter, O. (1991) J. Appl. Cryst. 24, 832–835.
[31] Glatter, O. (1993) J. Phys. IV 3, 27–38.
[32] Corti, M. (1985) in Physics of Amphiphiles: Micelles, Vesicles and Microemulsions (Degiorgio, V. and Corti, M., eds.), pp. 122–147, North-Holland, Amsterdam.
[33] Huang, C., Mason, J.T., Stephenson, F.A. and Levin, I.W. (1986) Biophys. J. 49, 587–595.
[34] Mushayakarara, E.C. and Mantsch, H.H. (1985) Can. J. Biochem. Cell Biol. 63, 1071–1076.
[35] Jain, M.K., Crecely, R.W., Hille, J.D.R., De Haas, G.H. and Gruner, S.M. (1985) Biochim. Biophys. Acta 813, 68–76.
[36] Mattai, J. and Shipley G.G. (1986) Biochim. Biophys. Acta 859, 257–265.
[37] Wu, W., Huang, C., Conley, T.G., Martin, R.B. and Levin, I.W. (1982) Biochemistry 21, 5957–5961.
[38] Wu, W. and Huang, C. (1983) Biochemistry 22, 5068–5073.
[39] Hui, S.W. and Huang, C. (1986) Biochemistry 25, 1330–1335.
[40] Arvidson, G., Brentel, I., Khan, A., Lindblom, G. and Fontell, K. (1985) Eur. J. Biochem. 152, 753–759.
[41] Eriksson, P.O., Lindblom, G. and Arvidson, G. (1987) J. Phys. Chem. 91, 846–853.
[42] Huang, C., Mason, J.T., Stephenson, F.A. and Levin, I.W. (1984) J. Phys. Chem. 88, 6454–6458.
[43] Isrealachvili, J.N. (1985) in Physics of Amphiphiles: Micelles, Vesicles and Microemulsions (Degiorgio, V. and Corti, M., eds.), pp. 38–49, North-Holland, Amsterdam.
[44] Hille, J.D.R., Gabrielle, M., Den Kelder, D., Sauve, P., De Haas, G.H. and Egmond, M.R. (1981) Biochemistry 20, 4068–4073.
[45] Small, D.M. (1986) in The Physical Chemistry of Lipids: From Alkanes to Phospholipids (Small, D.M., ed.), pp. 476–481, Plenum Press, New York.
[46] Pascher, I., Sundell, S., Eibl, H. and Harlos, K. (1986) Chem. Phys. Lipids 39, 53–64.
[47] Luzzatti, V. (1968) in Biological Membranes (Chapman, D., ed.), pp. 71–123, Academic Press, London and New York.
[48] Tardieu, A., Luzzatti, V. and Reman, F.C. (1973) J. Mol. Biol. 75, 711–733.